Coupling abundant active sites and Ultra-short ion diffusion path: R-VO_2/carbon nanotubes composite microspheres boosted high performance aqueous ammonium-ion batteries

Lin-bo Tang[1, 2#], Xian-kai Fan[1, 3#], Kai-xiong Xiang[4], Wei Zhou[1], Wei-na Deng[1], Hai Zhu[1], Liang Chen[1], Jun-chao Zheng[2]*, Han Chen[1]*

[1]School of Materials and Environmental Engineering, Changsha University, Changsha 410022, PR China

[2]School of Metallurgy and Environment, Central South University, Changsha, Hunan, 410083, China

[3]College of Energy Materials and Chemistry，Inner Mongonia University，Hohhot, Inner Mongolia, 011123, PR China

[4]Liling Ceramic Institute, Hunan University of Technology, Zhuzhou, Hunan, 412007, PR China

Corresponding author: jczheng@csu.edu.cn (j. c. Zheng); lzdxnchh@126.com (h. Chen).

#Lin-bo Tang and Xian-kai Fan contributed equally to this study.

1. Material Characterizations

The crystallographic characterizations were measured by X-ray diffraction (Bruker D8 Advance X-ray diffractometer; Cu Kα; λ = 0.152nm). Raman spectra were tested by a confocal Raman microscope (Renishaw Via Raman microscope; RM 1000-Invia; range of 100-2000 cm-1; λ=785 nm). The FT-IR spectra were analyzed by vertex-70 (Bruker; range of 400-4000 cm-1). Transmission electron microscopy (TEM), high-resolution transmission electron microscopy (TEM, JEOL-2100F, 200 kV) images were observed

with a microscope (JEM2100F STEM/EDS). Energy dispersive X-ray spectra (EDS) were collected by an EDS system (Oxford EDS IE250). Field emission scanning electron microcopy (FESEM) pictures were observed by a microscope (FE-SEM, JEOL JSM-7500F). X-ray photoelectron spectroscopy (XPS) was performed on an system equipped (Escalab 250Xi; monochromatic Al Kα; 1486.6eV). The contents of materials were determined using thermogravimetric analysis (TGA, Shimadzu DTG-60H).

2. Electrochemical Measurements

The cathodes were premier fabricated by making the slurry of 80 wt% R-VO_2 microspheres or R-VO_2/CNTs composite microspheres, 10 wt% acetylene black, and 10 wt% polyvinylidene fluoride (PVDF) and N-methyl pyrrolidone(NMP), the slurry was then spread on stainless steel (SUS 304) foil and dryed for 24 h at 80 °C in a vacuum oven.

The anodes were premier fabricated by making the slurry of 80 wt% active carbon or UP, 10 wt% acetylene black, and 10 wt% polyvinylidene fluoride (PVDF) and N-methyl pyrrolidone(NMP), the slurry was then spread on stainless steel (SUS 304) foil and dryed for 24 h at 80 °C in a vacuum oven.

Button battery (CR2016-type): The $(NH_4)_2SO_4$ aqueous solution of 0.5 mol L^{-1} was used as electrolyte and glass fiber film were used as separator. The CR2016 coin batteries were assembled in the dry atmosphere.

Three-electrode test system: The R-VO_2 microspheres, active carbon and Ag/AgCl electrode were respectively employed as the working electrodes, counter electrodes and

reference electrodes, and the 0.5 mol L^{-1} K_2SO_4, Na_2SO_4 and $(NH_4)_2SO_4$ aqueous solution were employed as the electrolytes.

The charge-discharge tests and the Galvanostatic Intermittent Titration Technique (GITT) were employed by means of NEWARE battery testing systems. Cyclic voltammetry (CV) and AC impedance (AC) were measured on an electrochemical workstation (CHI760E). All the tests are done at room temperature.

3. Density functional theory calculations

All calculations were based on density functional theory (DFT), using the Vienna ab initio Simulation Package (VASP) code. The exchange and correlation terms were described using general gradient approximation (GGA) in the scheme of Perdew-Burke-Ernzerhof (PBE). Core electrons were described by pseudopotentials generated from the projector augmented wave method, and valence electrons were expanded in a plane-wave basis set with an energy cutoff of 400 eV. The DFT+U method was employed to optimize the structure, in which the onsite parameter U_{eff} (= U – J) was chosen to be 4.2 eV for the V 3d electron. The relaxation is carried out until all forces on the free ions are converged to 0.01 eV/Å. A 2×2×2 VO_2 supercell ($V_{16}O_{32}$) was used to calculate the diffusion properties of cations. Climbing Image Nudged Elastic Band (CI-NEB) method was used to find the minimum energy paths and the transition states for diffusion of cations in VO_2, with a force converge < 0.01 eV/Å. During the CI-NEB calculation, all the structures are allowed to relax within the fixed lattice parameters.

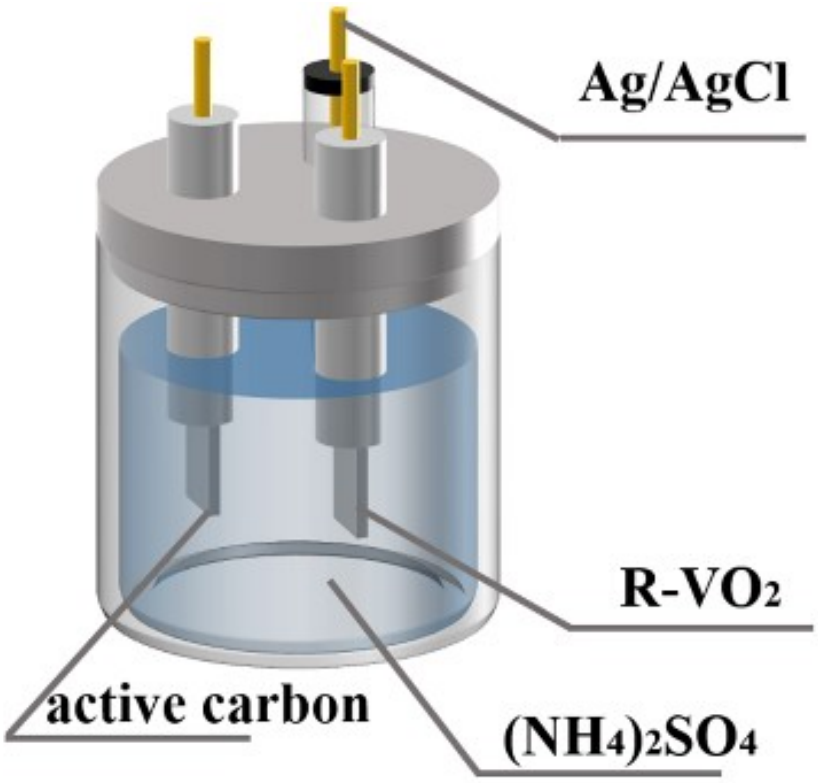

Figure S1. Schematic diagram of three-electrode test system

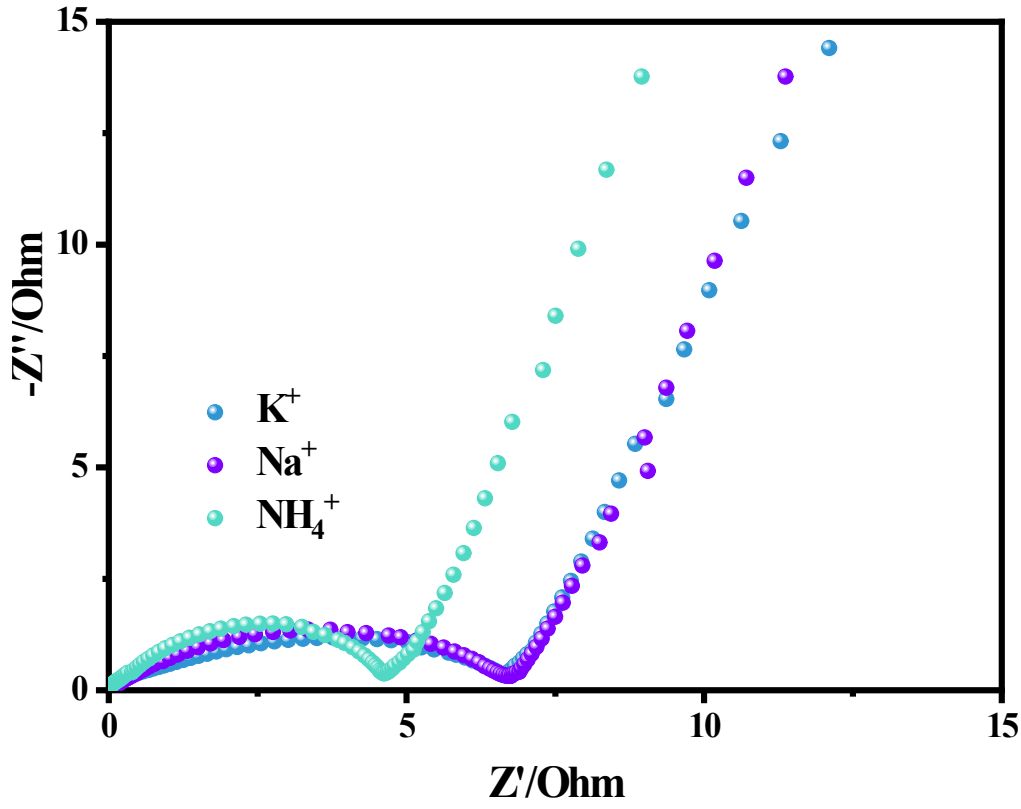

Figure S2. the electrochemical impedance spectroscopy (EIS) (c) for three charge carriers of K^+, Na^+, NH_4^+ ions

Figure S3. Cyclic voltammetry (CV) curves at various scan rates from 0.1 to 1.0 mV s^{-1} for K^+ (a) and Na^+ (d) to R-VO_2, log (i) versus log (v) curves of cathodic peaks for K^+ (b) and Na^+ (e), surface-controlled and diffusion-controlled contributions to capacity for K^+ (c) and Na^+ (f)

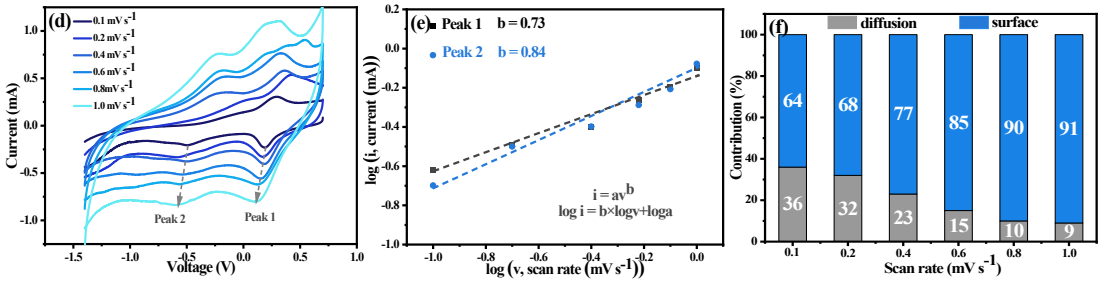

Figure S4. CV curves at various scan rates from 0.1 to 1.0 mV s^{-1} for R-VO_2 microspheres (a), log (*i*) versus log (*v*) curves of cathodic peaks for R-VO_2 microspheres (b), surface-controlled and diffusion-controlled contributions to capacity for R-VO_2 microspheres (c)

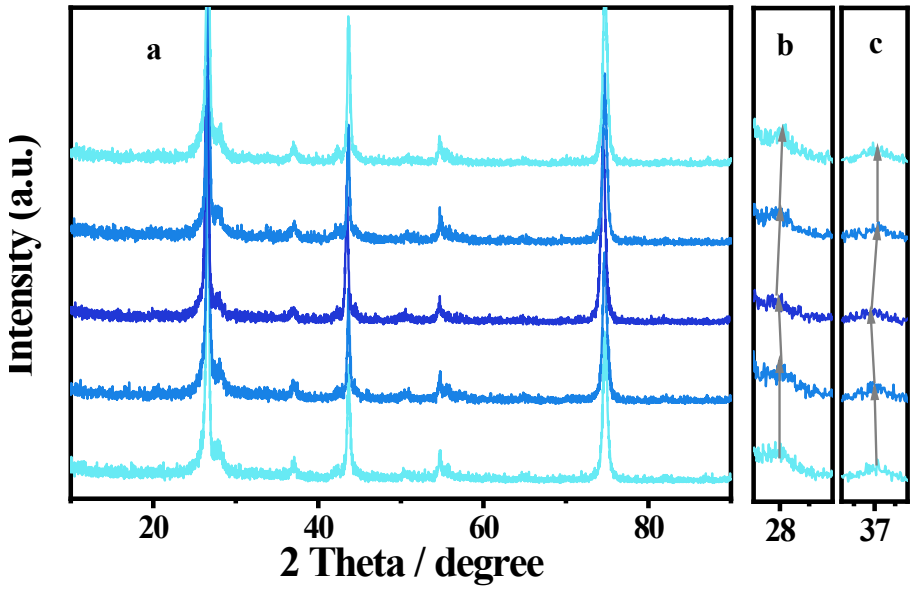

Figure S5. Ex situ XRD patterns of R-VO_2 microspheres

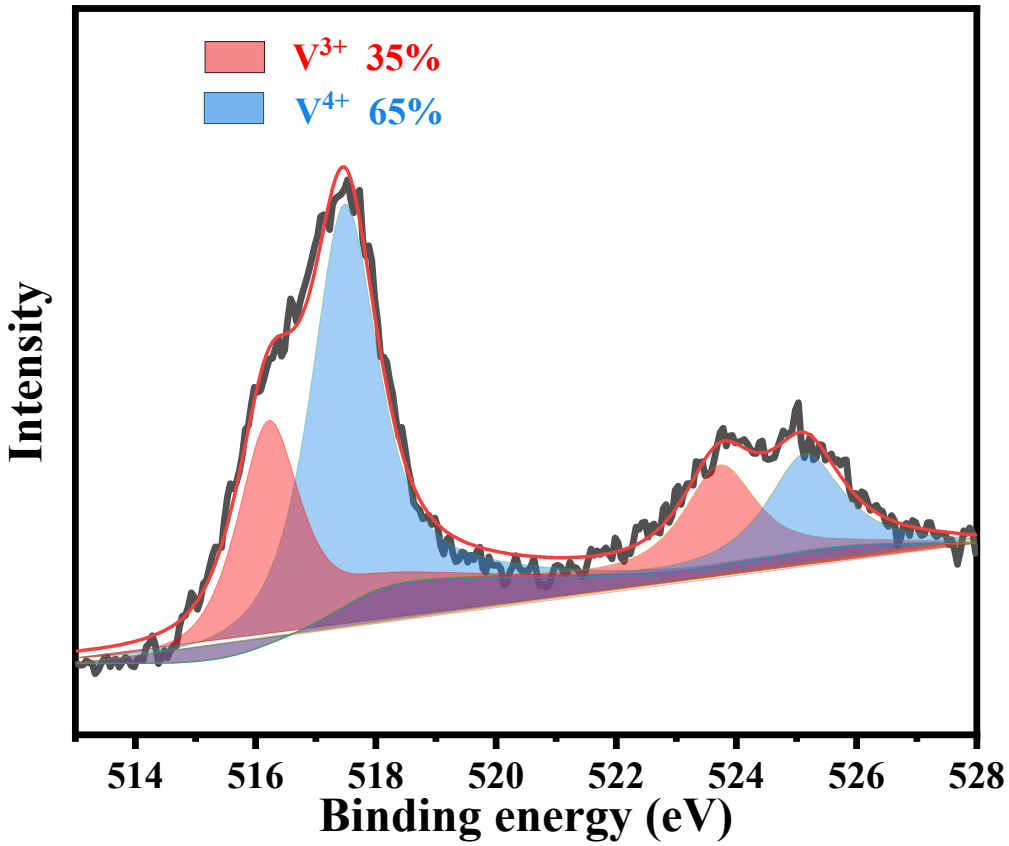

Figure S6. XPS patterns of R-VO_2 microspheres at discharged state

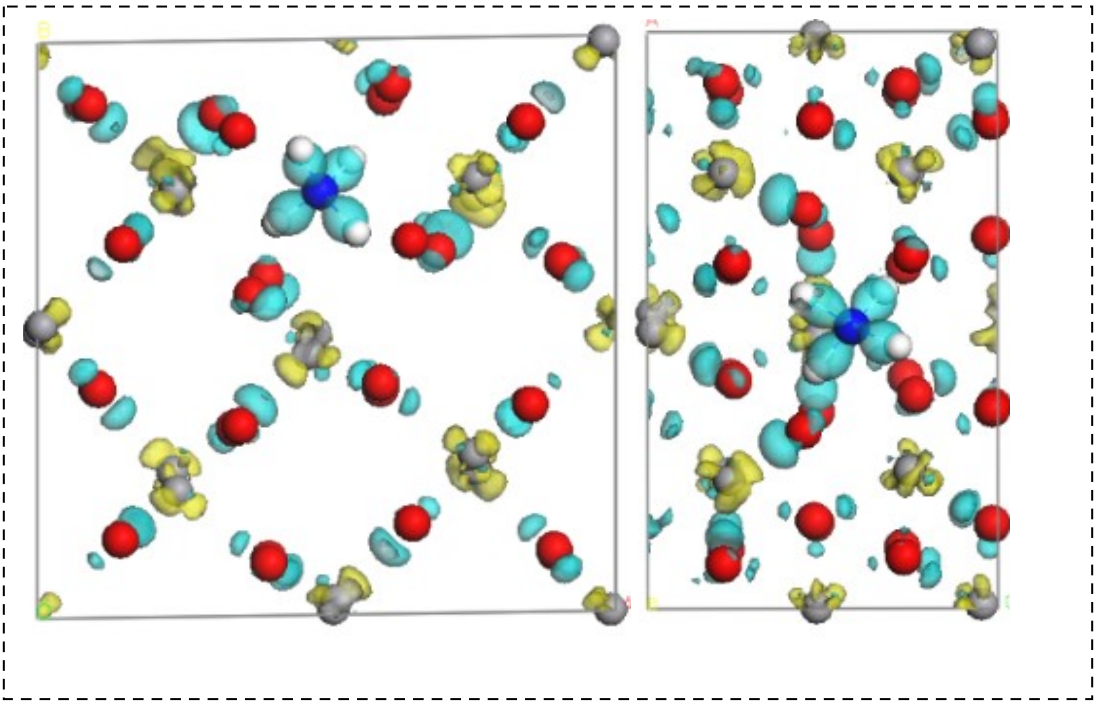

Figure S7. Diagram of charge density difference of NH_4^+ inserted R-VO_2

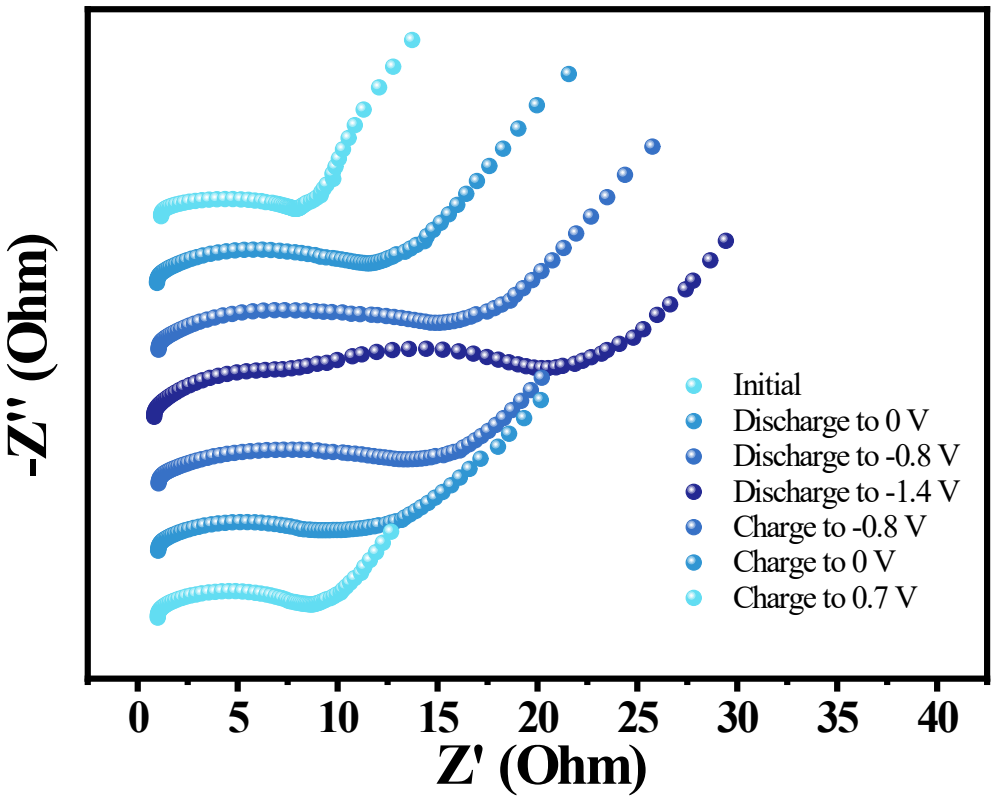

Figure S8. In situ electrochemical impedance of R-VO_2 microspheres during the first cycle

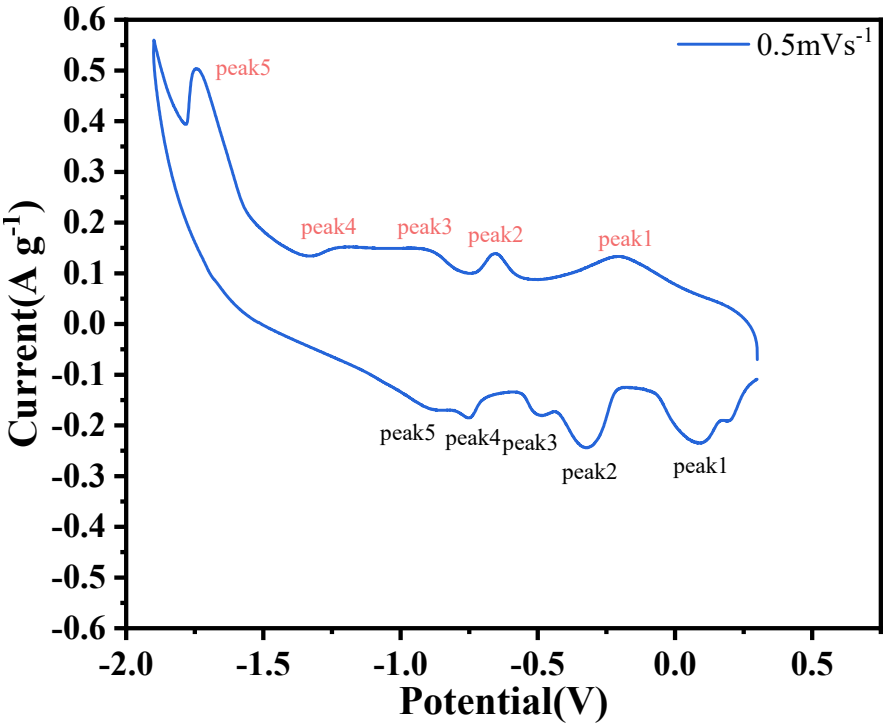

Figure S9. The CV curve of UP anode

Table S1. The fitting results of electrochemical impedance spectroscopy for two microspheres

	0.76883	0.83044
	2.281	3.869
	1.596 E-4	9.1621E-5
	0.8448	0.92097
	6.15	7.814
	0.1795	0.17622
	0.46131	0.51516

Table S2. The fitting results of in situ EIS for R-VO_2/CNTs composite microspheres

	0.76883	0.79217	0.8002	0.87252	0.79445	0.77114	0.71999
	2.281	3.272	3.96772	6.142	5.458	3.638	2.065
	1.596E-4	1.8464E-4	1.8826E-4	1.9623E-4	1.8963 E-4	1.7716E-4	1.5088E-4
	0.8448	1.062	1.12882	1.82005	0.80951	0.8058	0.78469
			10.28	10.76	10.15		
			0.0018795	0.005992	0.0039663		
			0.42882	0.85687	0.47827		
	6.15	6.564	9.73	12.2	11.342	5.96	5.622
	0.1795	1.141	2.1	2.892	2.223	0.255	0.20793
	0.46131	0.4724	0.51877	0.6643	0.6024	0.46516	0.45656